

Development of Silicon Photomultipliers and their Applications to GlueX Calorimetry

Elton S. Smith for the GlueX Collaboration^{1,a)}

¹Jefferson Lab, Newport News, VA 23606 USA.

^{a)}Corresponding author: elton@jlab.org

Abstract. The GlueX experiment is a photoproduction experiment in Hall D at Jefferson Lab that is being commissioned for use with the new 12 GeV accelerator. The purpose of the experiment is to search for Hybrid mesons, which are mesons with quark and gluon degrees of freedom. The barrel calorimeter of GlueX is instrumented with 4000 large-area (1.2 x 1.2 cm²) silicon photomultipliers (SiPMs). These photon sensors have properties similar to vacuum photomultipliers, but are unaffected by high magnetic fields. In our experiment they operate in magnetic fields exceeding 1T. After extensive tests with a variety of sensors, we chose the S12045(X) custom SiPM arrays manufactured by Hamamatsu Corporation, also known as multi-pixel photon counters (MPPCs). We will give an overview of this new technology as well as the experience gained during two commissioning periods with beam.

BACKGROUND

Jefferson Laboratory (JLab) operates the Continuous Electron Beam Accelerator Facility (CEBAF) and is located in Newport News, Virginia, USA. The accelerator has been recently increased the beam energy from 6 to 12 GeV to increase the kinematic reach of experiments exploring properties of nucleons and nuclei. The GlueX Experiment [1] is a key element of the Jefferson Lab 12 GeV upgrade. The experiment is at the end of a new beamline at the CEBAF accelerator complex at Jefferson Lab that will use 12 GeV electrons to deliver linearly-polarized photons to a new experimental area, Hall D. The primary physics goal of GlueX is to discover and study the properties of hybrid mesons – particles where the gluonic field contributes directly to the J^{PC} quantum numbers of the mesons [2]. Lattice QCD calculations indicate that several of the nonets of these hybrid mesons have exotic quantum numbers, forbidden J^{PC} for a simple fermion-antifermion system [3]. In addition, the detector has high efficiency for reconstruction for particles in the expected mass range for the lightest hybrids, which is below 3 GeV. The GlueX detector has been installed in the experimental hall and we have completed two short commissioning periods with beam. In late October to mid December 2014 data were collected with 10 GeV electrons, unpolarized photon beam and a solid target. In April 2015 we ran for a few days with 6 GeV electrons producing linearly-polarized photons on the liquid-hydrogen GlueX target. In total we collected about 2 billion events, corresponding to about 200 TB of data. All detector systems were checked and are operating within 30% of design specs. The first physics quality beam is expected in 2016. A review of the performance both in calibrating and understanding the detector can be found in Ref. [4].

GLUEX AND THE BARREL CALORIMETER

The GlueX detector is azimuthally symmetric and nearly hermetic for both charged particles and photons, and is shown schematically in Fig. 1. The detector is configured around a 2-T solenoidal magnet. For physics running, a linearly polarized photon beam impinges on a liquid hydrogen target and events are reconstructed by measuring charged tracks in the central and forward drift chamber systems and reconstructing showers from photons hitting the barrel (BCAL) and forward calorimeters. Particle identification is accomplished using energy loss measurements in the chambers and time-of-flight measurements in a hodoscope covering the forward calorimeter.

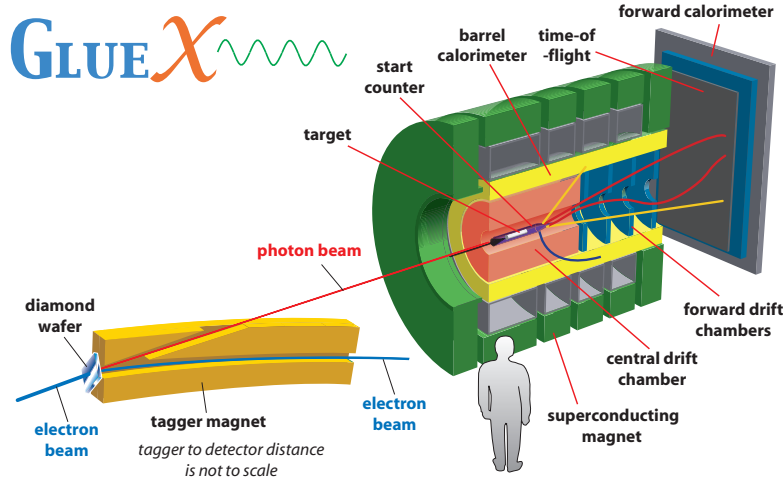


FIGURE 1. A schematic drawing of the Hall-D photon tagger and the GlueX detector at Jefferson Lab. The distance from the tagger to the detector, which is compressed in the figure, is about 100 m. The barrel calorimeter is colored in yellow.

The GlueX detector uses silicon photomultipliers (SiPMs) to detect the scintillation light produced in the barrel calorimeter, the start counter, the pair spectrometer and the tagging spectrometer microscope.¹ The SiPMs are also referred to as Multi Pixel Photon Counters (MPPCs). The sensitive area of SiPMs in GlueX is dominated by the sensors in the barrel calorimeter, which we describe here in a little more detail. The BCAL [5, 6, 7] surrounds the tracking chambers inside the solenoid. Fig. 2 is a sketch of the BCAL, which is a lead scintillating-fiber calorimeter with readout on both the upstream and downstream faces. For particles entering normal to the calorimeter face, the calorimeter is 14.9 radiation lengths thick. The BCAL is sensitive to photons between polar angles of 12° and 160° and π^0 have been reconstructed using photons of energy above 100 MeV. The expected energy resolution is $\sigma_E/E \approx 5.4\%/\sqrt{E/\text{GeV}} \oplus 2.3\%$ and the typical width of reconstructed π^0 mass for GlueX reactions is about 9 MeV. The BCAL is read out using both 250 MHz custom Flash ADCs [8] as well as 60 ps TDCs [9]. The timing information is used to provide time-of-flight information for particles interacting in the BCAL, and is used in the global particle identification methods for both charged particles and photons.

SILICON PHOTOMULTIPLIER ARRAYS

The selection of the optimum light sensor for a given detector depends on many factors including the properties of the sensors, geometrical constraints, cost, safety, and ease of use. It is particularly difficult to make direct cost comparisons between the two sensor types because the implementations of the two systems are so different. For example, SiPMs can be operated inside the magnetic field, which obviates the need for light guides and magnetic shielding that are needed for vacuum photomultiplier tubes (PMTs). On the other hand, SiPMs are very sensitive to temperature, which requires a temperature stabilization system unnecessary for PMTs. Also in order to cover the same sensitive area one requires less PMTs but also less electronic readout channels. Nevertheless, the chosen sensor must meet the basic detector requirements so we give a comparison of the typical characteristics of SiPMs relative to PMTs in Table 1. The advantages of the SiPMs are collected at the top part of the table and the advantages of vacuum PMTs are collected at the bottom. Neither sensor dominates in all categories. To date experience with large numbers of SiPMs in particle-physics experiments is limited, with the T2K experiment blazing the path with 53,000 $1.3 \times 1.3 \text{ mm}^2$ S10362-13-50C sensors used in their near detectors [10]. Other experiments are also considering this new technology, for example the Fermilab g-2 experiment [11]. Our selection of SiPMs as the light sensors for the BCAL was driven by their insensitivity to magnetic fields, which is about 1T at the sensor location. For this application, the development of relatively large area SiPM arrays ($\sim 1.44 \text{ cm}^2$) was critical, as only much smaller devices ($\sim 0.09 \text{ cm}^2$) had been

¹The pair spectrometer and tagging microscope systems are not shown in the figure. They are used to measure and monitor the characteristics of the polarized photon beam.

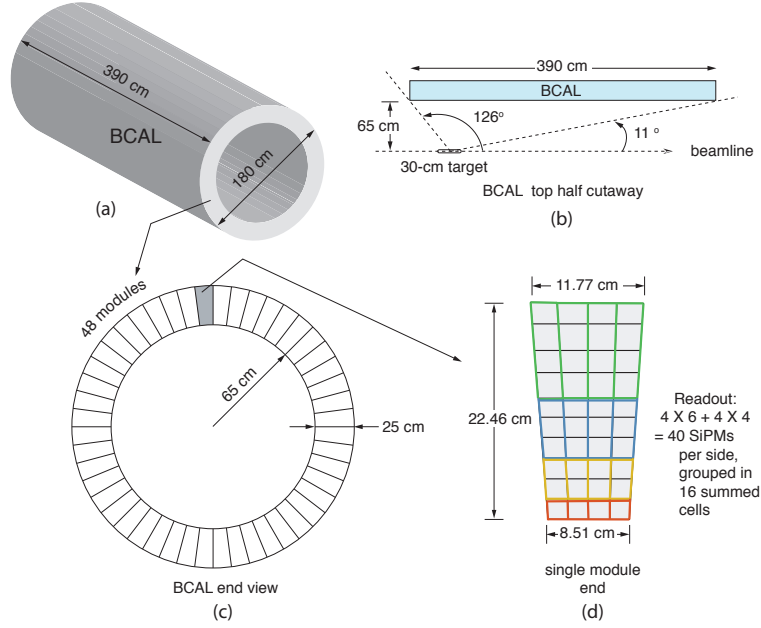


FIGURE 2. Sketch of BCAL. a) Dimensions of barrel. b) Side view of BCAL showing the location of the target. c) End view of the BCAL, showing the segmentation into 48 modules, each 390 cm long. d) End view of one module, showing the location of the 40 light sensors on one face.

available before 2010. We also determined that the high dark rate, which also increases with radiation damage, did not significantly impact our expected resolution. In addition, we developed a system to stabilize the temperature and thereby the gain, and cool the sensors to reduce the dark rate. In the sections that follow, we will review the process of testing and operational experience with these SiPMs.

TABLE 1. Typical characteristics for vacuum photomultipliers compared to those of SiPMs. The advantages of SiPMs are collected in the top part of the table.

Characteristic	Vacuum photomultiplier	SiPM
Bias voltage	1200 – 2500 V	$\sim 1V$ above $V_{br} \sim 70V$
Sensitivity to B fields	Yes	No
Single p.e. resolution	Medium	Excellent
Size	$\sim 5 \times 5 \times 15 \text{ cm}^3$	$\sim 1.5 \times 1.5 \times 0.5 \text{ cm}^3$
Quantum efficiency	$\sim 20\%$ (QE)	$\sim 20\%$ (PDE)
Gain	$10^2 - 10^8$, adjustable	10^6 , fixed within 50%
Area of sensor	1 – 500 cm^2	0.01 – 1 cm^2
Linearity	$\sim 1\%$	Depends on number of micro-cells
Sensitivity to radiation?	No	Increased dark rate
Dark current rate	$\sim \text{kHz} / \text{cm}^2$	$\sim 10 \text{ MHz} / \text{cm}^2$
Sensitivity to temperature?	No	Yes

Hamamatsu S12045(X) MPPC array

The SiPM chosen for our application was the Hamamatsu S12045(X) MPPC array, which is a 4×4 array of $3 \times 3 \text{ mm}^2$ cells. Each cell is composed of 3600 $50\mu\text{m}$ pixels. The array has 20 pins (see Fig. 3), four bias pins to power individual rows, and 16 outputs for the signals of each of the cells. The individual outputs were used during acceptance testing to check the signals from individual cells. However, for installation in the detector all four bias pins were connected

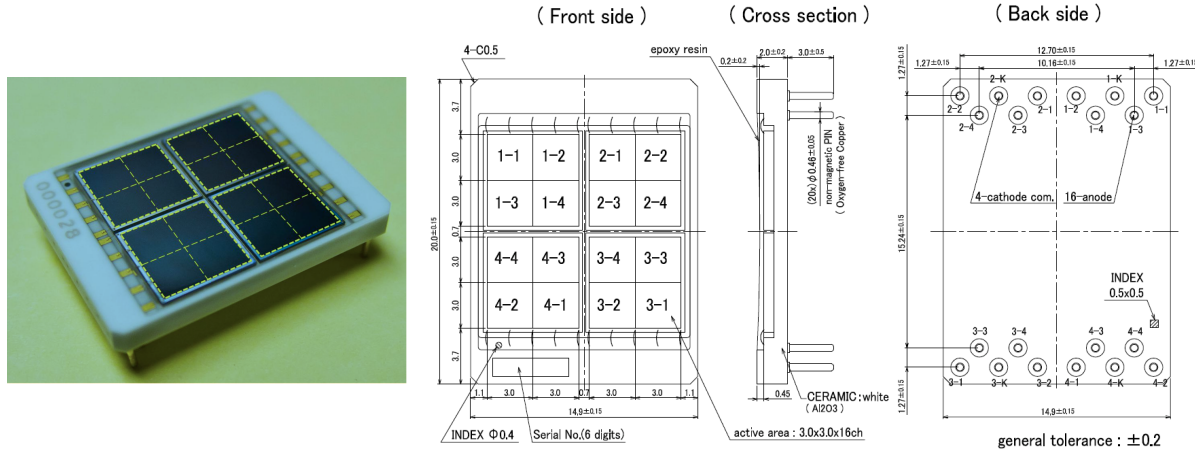


FIGURE 3. Left: photo of SiPM array Hamamatsu MPPC S12045(X) with dashed lines indicating the sensitive tiles. Right: Drawings of SiPM array. Note that the back side behind the active sensors is bare, which allows for direct cooling.

to a single input and the 16 output signals were joined to generate a single summed output for the array. Following the preamp stage, the outputs of each array were summed by columns in a 1-2-3-4 scheme as indicated by colors in Fig. 2d. This resulted in no summing for the beginning of the shower (layer 1), adding 2 sensors for layer 2, 3 sensors for layer 3 and 4 sensors for end tail of the shower (layer 4). This reduced the number of channels from a single module side with 40 SiPMs down to 16 signals, which were digitized using JLab 250 MHz Flash ADCs. Additionally, the signals from the inner three layers were discriminated and input to JLab F1 60 ps pipeline TDCs.

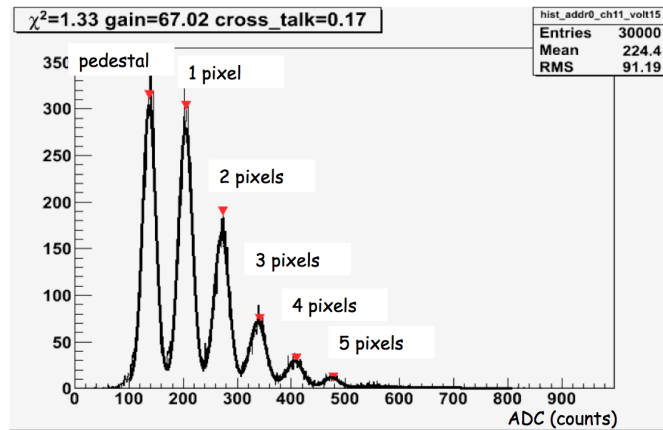


FIGURE 4. Example spectrum of SiPM response to very low light levels [12], which shows individual pixels firing. The y-axis is in counts.

The SiPM arrays were tested extensively before acceptance. Four thousand units were purchased and 3840 are installed in the detector. The testing was divided between two collaborating institutions: 30% at JLab [13] and 70% at the Universidad Técnica Federico Santa María (USM) [12, 15]. In total only four units failed specifications and were replaced by Hamamatsu. The testing was performed with separate and independent measuring equipment at the two institutions. JLab measured the response of each cell at its nominal operating voltage at a single temperature (15°C) to five different light levels from an LED source. The absolute light intensity of the LED source at the location of the sensors was determined using a Hamamatsu S2281 diode with unity gain and 100 mm² area, calibrated by the company. USM measured the response of each cell at three different temperatures (5, 7 and 20°C) at two different light levels and several voltage settings. These tests were supplemented at the University of Regina by measurements of the response of ten units to a realistic BCAL fiber spectrum. An example spectrum for one cell for one setting

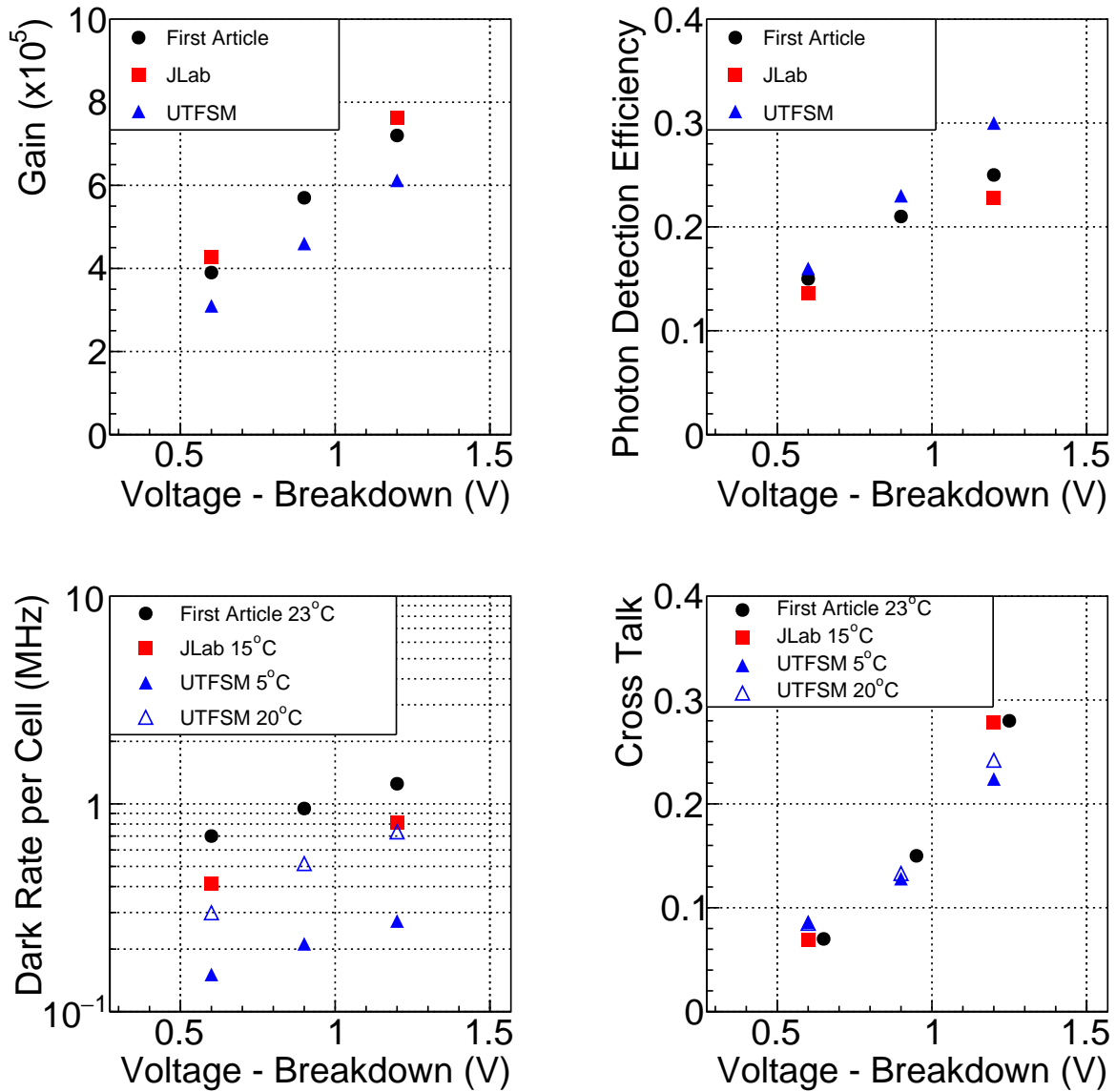


FIGURE 5. Measurements of the first-article samples (black circles) [13, 14], production samples at JLab (red squares) and production samples at UTFSM (triangles) [12, 15] of four basic SiPM parameters as a function of the voltage over breakdown. Top left) gain, Top right) photon detection efficiency, Bottom left) dark rate and Bottom right) cross talk. As long as the voltage over breakdown is kept constant, the dark rate dependence is the only variable that has a significant temperature dependence.

is shown in Fig. 4. At low light levels for testing, individual pixels firing are clearly visible, although the response to particles generates considerable more light. These spectra were used to determine gain, cross talk and dark rate under each of the test settings mentioned above. The photon detection efficiency (PDE) was also determined using the calibrated light source. A summary of the SiPM parameters is shown in Fig. 5.

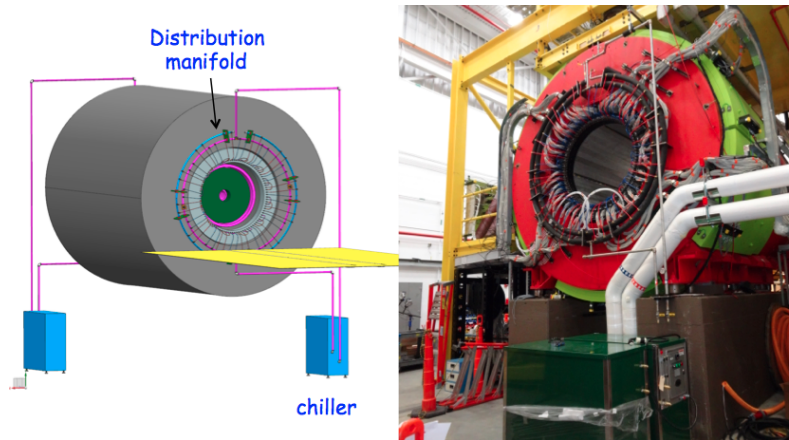


FIGURE 6. Left: Schematic of chiller and manifold connections. Right: Photo of chillers, manifold and connections to BCAL (inside solenoid) during testing and installation.

Temperature Stabilization

The gain of the SiPM depends on the voltage above the breakdown voltage (V_{br}), which is about 70 V for these sensors. The breakdown voltage has been determined to be a linear function of temperature over a broad temperature range [16] with a slope between 50 and 60 mV/°C. This imposes practical constraints on the operation of SiPMs if the gain is to be kept constant during operation. Our strategy is two-fold. First, we stabilize the temperature within practical limits ($\pm 2^\circ\text{C}$). Second, we stabilize the gain within the narrow temperature window using a negative-temperature-coefficient thermistor. Two chillers are installed, one to cool the upstream and one to cool the downstream ends of the BCAL. The coolant of the chillers is circulated via manifolds through copper pipes that are in thermal contact with a plate that cools the back side of the forty SiPMs on each module face through a silicon pad. The gain is then stabilized by adjusting the bias voltage using a negative coefficient thermistor, which is in contact with the cooling plate. See Fig. 6. During production running at high intensity, when we expect to see the effect of radiation damage, we plan to operate the sensors at 5°C . To date, the chillers have been operated reliably down to 10°C and the electronics is flushed with nitrogen to prevent condensation. With the chiller set to 10°C , the cooling plate temperatures range between $11\text{--}12^\circ\text{C}$ and the environment inside the electronics volume results in a temperature of about 21°C , 1–5% relative humidity and dew points less than -20°C .

Radiation damage

Silicon detectors generally deteriorate after exposure to radiation and SiPMs are no exception. An early irradiation test on SiPMs using a series of high activity Cs-137 sources at JLab showed that SiPMs are insensitive to electromagnetic radiation and there was no significant change in performance of SiPMs up to 2 krad of 0.7 MeV-gamma irradiation. But neutron radiation does cause damage and its effect was studied parasitically in an experiment at JLab and also systematically with a calibrated AmBe neutron source [17]. We studied the temperature dependence of the radiation damage and recovery on dark current and dark rate. The effect of neutron irradiation on the dark rate and pulse height is shown in Fig. 7. The dark current depends approximately linearly on the neutron fluence, but does not depend on the temperature or the operating voltage of the device. The pulse height remains relatively unchanged under neutron irradiation and the little change observed is recovered after a period of annealing. This feature is illustrated further in Fig. 8, where the dependence of dark current on the bias voltage (IV curve) is shown to remain unchanged after irradiation, even when the dark current has increased by a factor of 25.

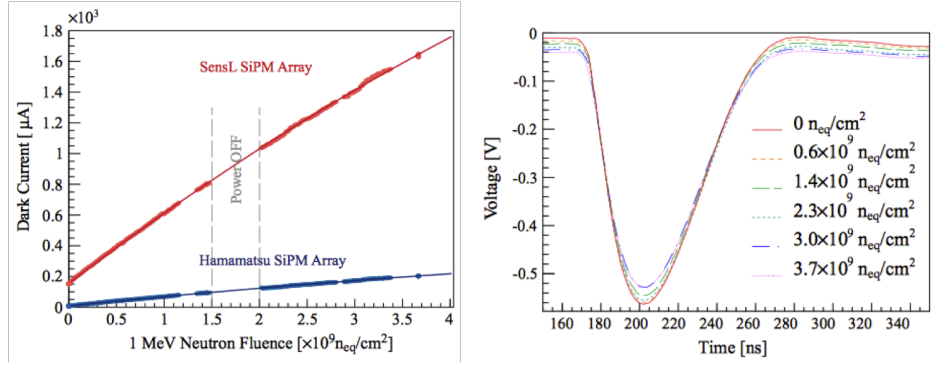


FIGURE 7. Left: Dark current vs neutron fluence for Hamamatsu and SensL sensors [17]. The dashed lines indicate the time when the devices were not powered. Right: Changes in pulse height following irradiation.

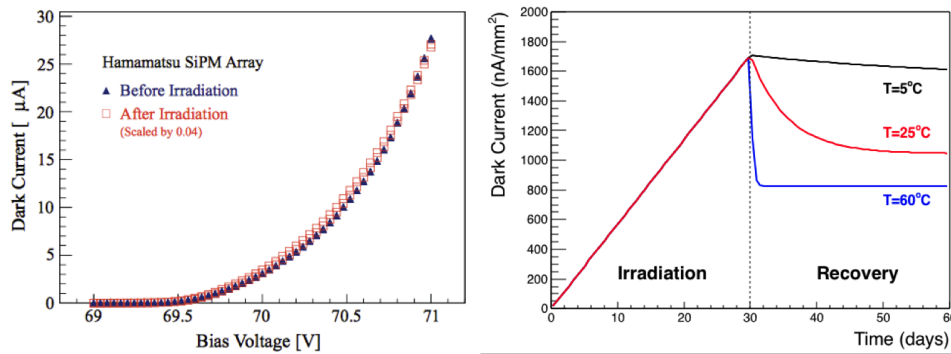


FIGURE 8. Left: Comparison of the I-V curve before and after irradiation [17]. After rescaling the dark rate for the irradiated sample, the curves coincide. Right: Illustration of the effect of annealing at different temperatures.

We also find that the SiPMs can anneal, which results in partial recovery of the acute damage induced by the neutron radiation. The speed and the extent of this annealing process strongly depends on the temperature and is faster and stronger at higher temperature. This process is illustrated in the right hand plot of Fig. 8 that shows an initial period of irradiation followed by a period of annealing at three different temperatures. At $T=5^{\circ}\text{C}$, the annealing time is 38 days and stabilizes at 90% of the maximum dark rate. At $T=25^{\circ}\text{C}$, the annealing time is 4.2 days and stabilizes at 61% of the maximum dark rate. Finally, at $T=60^{\circ}\text{C}$, the annealing time is 0.8 days and the dark rate comes down to 48% of the rate immediately following irradiation. We estimate that the dark rate per array will increase to 100 MHz, which is our specified maximum rate, after approximately 7 years of operation of high intensity production physics running in Hall D and operating at a temperature of 5°C with periodic annealing periods at 40°C . To date, we have accumulated a few weeks of running at low intensity beam, so we do not yet expect to observe any effects due to radiation.

SUMMARY

Silicon photomultipliers have been used successfully in a large-area application to calorimetry in the GlueX detector in Hall D at Jefferson lab. All SiPM sensors have exceeded our specifications. The system for gain stabilization is working as designed. Effects of radiation damage will be monitored as additional data is accumulated. The barrel calorimeter is performing close to specifications as shown by the reconstruction of 2-photons in Fig. 9 [4].

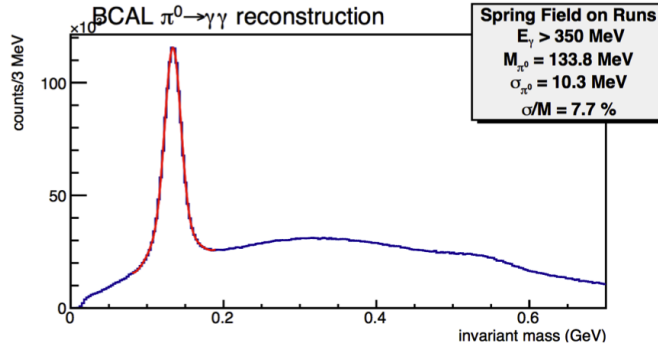


FIGURE 9. Reconstructed 2-photon mass distribution in the BCAL with preliminary calibrations and photon energies greater than 0.35 GeV. The π^0 mass peak is clearly visible. The half-width of the peak is $\sigma=10.3$ MeV, only slightly wider than our design goal.

ACKNOWLEDGMENTS

The authors thank the staff and administration of the Thomas Jefferson National Accelerator Facility who made this experiment possible. This material is based upon work supported by the U.S. Department of Energy, Office of Science, Office of Nuclear Physics under contract DE-AC05-06OR23177.

REFERENCES

- [1] The GlueX Collaboration, The GlueX Experiment in Hall D, 2010, Presentation to JLab PAC 36, http://www.gluex.org/docs/pac36_update.pdf.
- [2] C. A. Meyer and E. S. Swanson, Prog. Part. Nucl. Phys. **82**, 21–58 (2015).
- [3] J. J. Dudek *et al.* (Hadron Spectrum), Phys. Rev. **D88**, p. 094505 (2013).
- [4] C.A. Meyer *et al.* (GlueX), “First Results from The GlueX Experiment,” in *16th International Conference on Hadron Spectroscopy (Hadron 2015) Newport News, Virginia, USA, September 13-18, 2015* (2015) arXiv:1512.03699 [nucl-ex].
- [5] B. Leverington *et al.*, Nucl. Instrum. Methods **A596**, 327–337 (2008).
- [6] Z. Papandreou, B. Leverington, and G. Lolos, Nucl. Instrum. Methods **A596**, 338–346 (2008).
- [7] A. Baulin *et al.*, Nucl. Instrum. Methods **A715**, 48–55 (2013).
- [8] B. Barbosa *et al.*, “A VME64x, 16-Channel, Pipelined 250 MSPS Flash ADC With Switched Serial (VXS) Extension,” Tech. Rep. GlueX-doc-**1022** (Jefferson Lab, 2008).
- [9] B. Barbosa *et al.*, “The Jefferson Lab High Resolution Time-to-Digital Converter (TDC),” Tech. Rep. GlueX-doc-**1021** (Jefferson Lab, 2008).
- [10] M. Yokoyama *et al.* (T2K), Nucl. Instrum. Methods **A622**, 567 – 573 (2010).
- [11] A. Fienberg *et al.* (g-2), Nucl. Instrum. Methods **A783**, 12 – 21 (2015).
- [12] O. Soto *et al.*, Nucl. Instrum. Methods **A732**, 431–436 (2013).
- [13] F. Barbosa *et al.*, Nucl. Instrum. Methods **A695**, 100 – 104 (2012).
- [14] B. Barbosa *et al.*, “Test Results for the 80 First Article samples of the Hamamatsu S10943-0258(X) array,” Tech. Rep. GlueX-doc-**1777** (Jefferson Lab, 2011).
- [15] O. Soto *et al.*, Nucl. Instrum. Methods **A739**, 89–97 (2014).
- [16] P. Lightfoot *et al.*, JINST **3**, p. P10001 (2008), arXiv:0807.3220 [physics.ins-det].
- [17] Y. Qiang *et al.*, Nucl. Instrum. Methods **A698**, 234 – 241 (2013).